1642–1656 *Nucleic Acids Research, 2016, Vol. 44, No. 4* *Published online 8 November 2015*
doi: 10.1093/nar/gkv1162

Binding of 14-3-3 reader proteins to phosphorylated DNMT1 facilitates aberrant DNA methylation and gene expression

Pierre-Olivier Estève[1,†], Guoqiang Zhang[1,†], V.K. Chaithanya Ponnaluri[1], Kanneganti Deepti[1], Hang Gyeong Chin[1], Nan Dai[1], Cari Sagum[2], Karynne Black[2], Ivan R. Corrêa, Jr.[1], Mark T. Bedford[2], Xiaodong Cheng[3] and Sriharsa Pradhan[1,*]

[1]New England Biolabs Inc, 240 County Road, Ipswich, MA 01938, USA, [2]Department of Epigenetics and Molecular Carcinogenesis, The University of Texas MD Anderson Cancer Center, Smithville, TX 78957, USA and [3]Department of Biochemistry, Emory University School of Medicine, Atlanta, GA 30322, USA

Received August 11, 2015; Revised October 19, 2015; Accepted October 21, 2015

ABSTRACT

Mammalian DNA (cytosine-5) methyltransferase 1 (DNMT1) is essential for maintenance methylation. Phosphorylation of Ser143 (pSer143) stabilizes DNMT1 during DNA replication. Here, we show 14-3-3 is a reader protein of DNMT1pSer143. In mammalian cells 14-3-3 colocalizes and binds DNMT1pSer143 post-DNA replication. The level of DNMT1pSer143 increased with overexpression of 14-3-3 and decreased by its depletion. Binding of 14-3-3 proteins with DNMT1pSer143 resulted in inhibition of DNA methylation activity *in vitro*. In addition, overexpression of 14-3-3 in NIH3T3 cells led to decrease in DNMT1 specific activity resulting in hypomethylation of the genome that was rescued by transfection of *DNMT1*. Genes representing cell migration, mobility, proliferation and focal adhesion pathway were hypomethylated and overexpressed. Furthermore, overexpression of 14-3-3 also resulted in enhanced cell invasion. Analysis of TCGA breast cancer patient data showed significant correlation for DNA hypomethylation and reduced patient survival with increased 14-3-3 expressions. Therefore, we suggest that 14-3-3 is a crucial reader of DNMT1pSer143 that regulates DNA methylation and altered gene expression that contributes to cell invasion.

INTRODUCTION

DNA methylation at cytosine residues in the mammalian genome plays an important role in gene expression and development. Methylated CpGs in the promoter are thought to suppress the binding of transcription factors, thus controlling gene expression. Discovery of several repressor proteins that bind methylated DNA, specifically methyl-CpG binding domain (MBD) proteins, have been shown to relay the methylation information into appropriate functional state of the chromatin. The precise spatial and temporal regulation of gene transcription by appropriate DNA methylation is of vital importance during mammalian development, including X-chromosome inactivation, and genome stability (1,2). DNA methylation patterns are faithfully inherited during both mitosis and meiosis. Genome wide studies have demonstrated that while some CpG regions are stably methylated, a small number of CpGs remain dynamically methylated. These regions are speculated to play a major role in controlling the transcription network of the cells (3). Failure to target and preserve methylation of the correct DNA sequence often results in aberrant DNA methylation, which is a hallmark of cancer (4). In cancer cells, although the genome is hypomethylated in general, a large number of tumor suppressor genes are hypermethylated and transcriptionally silenced (5,6).

Responsibility of maintaining the correct methylation pattern lies with the DNA (cytosine-5) methyltransferases (DNMTs), a family of proteins including DNMT1, DNMT3A and DNMT3B (7). Studies in the past have discovered a number of facilitator proteins that are required for the maintenance of DNA methylation. Loss of these proteins, for example DNMT3-like protein (DNMT3L), ubiquitin like containing PHD and RING finger domain protein 1 (UHRF1), and CXXC finger protein 1 (CFP1) lead to hypomethylation of the genome (8–11). Studies on methylation preservation by DNMT1 demonstrated its recruitment to the replication fork by proliferative cell nuclear antigen (PCNA) and specifically to hemimethylated site by UHRF1 (8,11,12). Thus, cooperation between DNMT1 and UHRF1 at the site of DNA replication is a crucial event

*To whom correspondence should be addressed. Tel: +1 978 380 7227; Fax: +1 978 921 1350; Email: pradhan@neb.com
†These authors contributed equally to the paper as first authors.

for epigenome inheritance. Apart from protein partners, RNAs are also shown to be modulators of DNA methylation by direct binding to DNMTs (13,14).

Another layer of surveillance of DNA methylation inheritance comes from post-translational modification of DNMTs, specifically on enzyme stability and/or activity in the cells (15–17). Protein phosphorylation is crucial in many cellular processes that can control protein–protein interactions, enzymatic activities, and subcellular localization (18). It also creates binding site for a family of protein known as 14-3-3. The family of 14-3-3 represents seven different types encoded by different genes in mammals. The main feature of the 14-3-3 proteins is their ability to bind a multitude of functionally diverse signaling proteins, including kinases, phosphatases, and transmembrane receptors. Phosphorylation of Cdc25C by CDS1 and CHK1 creates a binding site for 14-3-3ϵ type, and this results in sequestering of phosphorylated Cdc25C in the cytoplasm and preventing it from interacting with CycB-Cdk1 that are in the nucleus during G2/M transition (19,20). Furthermore, phosphorylation mark on histone H3S10 is read by 14-3-3 that facilitates transcriptional activation in collaboration with H3K9 and H3K14 acetylation during cell cycle (21). Thus, 14-3-3 reader proteins participate in both cellular signaling processes and epigenetic gene regulation.

During the DNA synthesis phase of the cell division, DNMT1 is needed to copy methylation pattern from the parental strand onto the newly synthesized daughter strand. The majority of the replication machinery-associated DNMT1 is phosphorylated by AKT1 kinase at the Ser143 (15). The phosphorylated species appear to be resistant to ubiquitin-mediated degradation. After S phase, DNMT1 is methylated at the adjacent Lys142 by the protein lysine methyltransferase SET7, and either subsequently ubiquitinated for degradation by proteasome pathway (22) or recognized by a methyl-reader protein PHF20L1 to localize DNMT1 in the perinucleolar space (23). Moreover, overexpression of PHF20L1 abolished ubiquitination of DNMT1Lys142me1 (23), suggesting the fate of DNMT1 strongly depends on the interplay between the writers (AKT1, SET7) and the methyl reader (PHF20L1) that interact with DNMT1 Lys142-Ser143 sequence. Therefore, further understanding of the dynamic interaction between reader, writer and eraser in DNMT1 function and stability is warranted. Here we show a phosphorylation reader protein, 14-3-3, which recognizes phosphorylated Ser143 in DNMT1, resulting in inhibition of DNMT1 activity, aberrant DNA methylation and cell invasion.

MATERIALS AND METHODS

Protein-domain peptide arrays

Biotin-labeled DNMT1pSer143 peptides were bound and detected by a protein-domain microarray as described previously (24). For this study, a new protein domain microarray was generated harboring GST fusion proteins/protein domains consisting of 86 different phospho-serine/-threonine binding motif. The protein-domain array contains GST fusions of WW, FF, 14-3-3, FHA, and BRCT domains, as well as POLO boxes (Supplementary Figure S1A).

Cell culture, treatment and stable clone generation

HEK293, NIH3T3, COS7 and HeLa cells were cultured in DMEM media supplemented with 10% serum. 14-3-3 isoforms were cloned into p3xFLAG-CMV-10 vector (Sigma-Aldrich). NIH3T3 stable cell line overexpressing 14-3-3 isoforms were generated by selecting the cells transfected with 14-3-3 constructs in 800 μg/ml of G418. After a week in culture, single colonies were picked up and verified by western blotting using anti-FLAG antibody.

For 5mC rescue experiment, EP10 and EP12 clones were transfected twice with a plasmid encoding for Ds-Red-DNMT1 using Fugene HD (Active Motif).

Cell synchronization experiments were performed using the double thymidine method. Cells were treated with two rounds of 2 mM thymidine for 16 h with 1× phosphate bufferedsaline (PBS) wash between both treatments and release into fresh media for 8 h. After the second thymidine treatment, cells were washed with 1× PBS and sampling was done at desired time points up to 24 h. Cell cycle progression was monitored using anti-Cyclin A antibody (sc-751, Santa Cruz Biotechnology).

GST-pull down assays

14-3-3 isoforms were cloned into the pGEX-5X-1 vector (GE Healthcare) and GST-tagged proteins were purified using Glutathione Sepharose beads (GE Healthcare). Sepharose beads containing 10 μg of 14-3-3 protein were incubated with 500 ng of recombinant baculovirus expressed DNMT1, which is phosphorylated at the Ser143 site (25). Protein bound to the beads was resolved by SDS-PAGE. DNMT1 was visualized by western blotting and bound protein was quantified by densitometry. In some cases, different amounts of DNMT1 were pre-incubated with protein phosphatase (PP1) (New England Biolabs) for 1 h per the manufacturer's instructions and then pulled-down by GST-14-3-3.

A N-terminal fragment of DNMT1 (1–446) tagged with GST was overexpressed in *E. coli* and purified as described previously (22). GST-DNMT1 (1–446) was phosphorylated by AKT1 (14-627, Millipore) with or without ATP. Then different amounts of recombinant 14-3-3 with a MBP tag were pulled-down by GST-DNMT1 fragment. GST-DNMT1 fragment and 14-3-3 were detected by western blotting using antibody recognizing DNMT1pSer143 and MBP tag, respectively.

For DNMT1pSer143 dephosphorylation protection assays by 14-3-3, different amounts of DNMT1 were pre-incubated with GST-14-3-3 followed by the addition of PP1 (New England Biolabs). Residual DNMT1pSer143 was detected using an anti-serum specifically recognizing DNMT1pSer143 (New England Biolabs). For *in vivo* assays, COS7 cells were co-transfected with plasmid encoding for DsRed-DNMT1, FLAG-14-3-3ϵ and Myc-MirAKT.

DNA methyltransferase assays

DNA methyltransferase assays were carried out as described previously (25). For on-bead DNMT1 inhibition assays, saturating amount of sepharose beads bound to either GST or GST-14-3-3γ were incubated overnight with

end over end rotation at 4°C with purified DNMT1 or DNMT1Δ580. Following this, methylation reaction was performed using hemimethylated substrate and tritiated AdoMet for 30 min at 37°C. For methylation assays using crude cell extract, 10 μg of crude extract was incubated with 100 ng of hemimethylated DNA in the presence of 1 μg RNase A for 30 min. Filter disc method was used to process the samples and the [^{3}H]CH_3 incorporated into the DNA was determined using liquid scintillation counter.

Immunoprecipitation and immunofluorescence

Immunoprecipitation and immunofluorescence were carried out as described previously (26,27). For the co-IP of DNMT1 and 14-3-3 in HEK293 cells, 100 μg of the nuclear extract was incubated with 2 μg anti-DNMT1 antibody (sc-20701, Santa Cruz) or anti-14-3-3γ antibody (sc-398423, Santa Cruz). IP reactions were blotted with anti-DNMT1 (M0231S, New England Biolabs), anti-14-3-3γ (5522S, CST) and anti-14-3-3ϵ (9635S, CST) antibodies as per the manufacturer's dilution recommendations. Co-IP of 14-3-3ϵ with DNMT1 in NIH3T3 stable cell lines overexpressing 14-3-3ϵ was carried out using the anti-FLAG antibody (F3165, Sigma-Aldrich). IP reactions were blotted with anti-DNMT1 antibody (sc-20701, Santa Cruz) or the same anti-14-3-3 antibody as those used in the HEK293 experiment. Normal IgG was used for control in all IP reactions. For immunoprecipitation of 14-3-3 from synchronized EP12, cells cross-linked with formaldehyde were sonicated and centrifuged to obtain supernatant containing soluble DNMT1. Five hundred microgram of this supernatant was incubated with 10 μg anti-FLAG antibody (F3165, Sigma). IP reactions were blotted with anti-DNMT1 antibody (ab87654, Abcam) and anti-14-3-3ϵ (9635S, CST).

For the detection of DNMT1 and 14-3-3 colocalization, COS7 cells were grown on coverslips and co-transfected with DsRed-DNMT1 and 3xFLAG-14-3-3 plasmids. DsRed-DNMT1 was visualized with an excitation wavelength of 594 nm, epitope tagged 14-3-3 was detected by mouse anti-FLAG antibody (F3165, Sigma-Aldrich) and visualized with an anti-mouse IgG coupled with Alexa Fluor 488 dye (Molecular Probes). In some cases, cells were co-transfected with DsRed-DNMT1S143A and CFP-14-3-3 isoforms. For the detection of DNMT1pSer143, cells were incubated with anti-serum recognizing DNMT1pSer143 (New England Biolabs) and visualized with an anti-rabbit IgG coupled with Alexa Fluor 488 dye. CFP-14-3-3 was visualized with an excitation wavelength of 405 nm. DNMT1pSer143 anti-serum (1/10000 dilution) blocked with DNMT1pSer143 peptide served as a control. DAPI was used for nuclear staining.

Gene knockdown using siRNA

For 14-3-3ϵ gene knockdown, HeLa cells were transfected with 30 nM of esiRNA (EHU105911, Sigma-Aldrich) or control esiRNA targeting EGFP (EHUEGFP, Sigma-Aldrich) for 48 h. RNAiFecT was used as a transfection reagent according to manufacturer's recommendations (Qiagen).

Global 5mC level quantification

One microgram genomic DNA was denatured at 98°C for 3 min, incubated on ice for 3 min and digested to single nucleosides using 1 μl of a proprietary blend of nuclease(s) and phosphatase(s) (New England Biolabs) in 80 μl volume at 37°C overnight. 5mC was quantified using LC/MS as described previously (23).

Genome-wide DNA methylation analysis

Genome-wide DNA methylation analysis was carried out using the Reduced Representation Bisulfite Sequencing method (28). 1 μg of genomic DNA from stable clones overexpressing 14-3-3ϵ or control vector was digested with MspI, end-repaired and dA-tailed according to manufacturer's conditions (New England Biolabs). Methylated NEB Illumina loop adaptor was ligated to the digested DNA (E7370S, New England Biolabs). Ligation product was size-selected for 150–400 bp fragments on 2% agarose gels and bisulfite converted using the EZ DNA Methylation Kit (Zymo Research). Libraries were enriched by PCR using EpiMark Hot Start Taq DNA Polymerase (New England Biolabs) and sequenced on the Illumina GAII platform with 72 bp paired-end reads. Libraries were made and sequenced using two independent clones.

Adaptor and low quality sequences (Phred score < 20) were trimmed from RRBS reads using the trim_galore package (http://www.bioinformatics.babraham.ac.uk/projects/trim_galore/) with the parameter of -RRBS -paired. Reads were mapped to the mouse reference genome mm10 using Bismark with Bowtie2 (29). CpG methylation was extracted from uniquely mapped reads using Bismark methylation extractor with the parameter of -p –no_overlap. Differential methylation analysis was carried out using the methylKit package (30), where logistic regression test was implemented on single CpG sites or genomic region sliding windows (window size 5 kb, step size 5 kb). The p-value of differential methylation test was corrected to *q*-values using the sliding linear model method. CpG sites or genomic regions with *q*-values < 0.01 were considered significantly differentially methylated.

Differential methylation analysis on genomic elements

Differential methylation on gene elements (−5 kb of transcription start site (TSS)∼ +5 kb of transcription termination (Ter), promoter, 5′ UTR, coding exon, intron, 3′ UTR) was calculated using a fixed-length bin method. Briefly, the coordinates of the gene elements were downloaded from the UCSC refseq table, significantly differentially methylated CpG sites obtained from methylKit were mapped to the gene elements using BEDTools (31), and then the elements were divided into 30 equal-length bins. The CpG methylation value of each bin was calculated by taking the median of methylation level of all CpG sites in that bin.

Tracks for mm10 repetitive elements and CpG islands were downloaded from UCSC table browser. Promoter (−2 kb ∼ TSS), gene body, terminator (transcription termination site ∼ +2 kb) and desert CpG islands were obtained by intersecting the CpG island track with those gene elements in the refseq table. Differential methylation on repet-

itive elements and CpG islands were calculated using the same method as that of gene elements.

RNA-seq analysis

RNA-seq libraries were constructed using the NEBNext® Ultra™ Directional RNA Library Prep Kit (New England Biolabs) per the manufacturer's instructions. Average insert size of libraries was 200 bp. Libraries were sequenced in 76 bp paired-end read mode on the Illumina NextSeq 500 platform.

Sequencing reads were mapped to mm10 using TopHat2 (−r 60 –library-type fr-firststrand) with a known transcriptome file supplied (UCSC 23 May 2014) (32). The number of reads mapped to each known gene were counted using htseq-count tools (−t exon −s reverse −i gene_id) and analyzed with DESeq2 (33,34), where a negative binomial generalized linear model test is implemented on raw counts. The p-value of differential expression was corrected using Benjamini-Hochberg adjustment method and adjusted *P*-value was obtained. Genes with adj *P*-value < 0.01 were considered significantly differentially expressed. Sample distance was calculated using Euclidean distance on the rlog-transformed counts. Heatmap were generated using the *Z*-scored-transformed rlog values of significantly changed genes.

Gene ontology analysis was carried out using the AmiGO 2 tools (35). Multiple comparisons were corrected using Bonferroni correction.

Correlation of DNA methylation and gene expression change

Differential methylation analysis was carried out in the context of promoter (−2 kb ∼ TSS) and gene body using methylKit, where all CpG sites in the promoter or gene body region commonly covered by the control and epsilon libraries were added up and subjected to logistic regression test. Only genes with significant expression change (adj *P*-value < 0.05) and significant methylation change (*q*-value < 0.05) were included in the association studies. Log_2 fold changes in gene expression were correlated to differential methylation value using Spearman's rank correlation. The correlation efficient and *P*-value were calculated using the cor.test function in R. When plotting the correlation data, a linear regression curve was also drawn.

Correlation studies were also carried out on representative genes. The normalized read coverage in RNA-seq (RPM, read per million) and methylation level of significantly methylated CpG sites was visualized using the Gviz package from the Bioconductor repository.

For correlation of 14-3-3 expression and DNA methylation in breast cancer, level 3 data of RNA-seq Ver2 and Illumina Infinium 450K array of 896 patients were retrieved from TCGA (http://cancergenome.nih.gov/, Breast Invasive Carcinoma). The methylation level of CpG sites (beta value) was mapped to different genomic elements, such as CpG island, LINE, SINE, LTR and satellite. The average beta value of all mapped CpG sites was calculated and used as the CpG methylation level of an individual patient. The 14-3-3ζ expression levels (measured in transcripts per million, TPM) in each patient were correlated with the CpG methylation level using Pearson correlation.

Quantitative PCR analysis of gene expression

Total RNA was extracted using Trizol reagent (Invitrogen) from NIH3T3 clones overexpressing 14-3-3ϵ or control vector. One microgram of total RNA was reverse transcribed to cDNA using ProtoScript II First Strand cDNA Synthesis Kit (New England Biolabs) and 40 ng cDNA was subjected to real-time PCR analysis using SYBR Green Supermix (Bio-Rad). The following primers were used: Cxcl12_F ACCAGTCAGCCTGAGCTACC, Cxcl12_R TAATTTCGGGTCAATGCACA; Synpo_F TCCTTCTCCACCCGGAAT, Synpo_R AGGGGGACATTGGTGGAG; Rgcc_F AGCGCCACTTCCACTATGAG, Rgcc_R CTGGAGAGGAGTTGGTTGGA; Dnaja4_F GACCCTGGCGATGTGATAAT, Dnaja4_R CTTCAGGTCCCCATGCTTTA; Zhx1_F TGTGAAGCGGAAGCTTTCTAA, Zhx1_R TTGGCACAACATCAAGTTCC; Thbs1_F CGTTTACAACGTGGACCAGA, Thbs1_R CGAACAGGCCTAGTCTACCG; Gapdh_F TGATGACATCAAGAAGGTGGTGAAG, Gapdh_R TCCTTGGAGGCCATGTAGGCCAT. Gene expression change was calculated using the $2^{-\Delta\Delta Ct}$ method.

Cell invasion assay

Invasiveness of the clones was evaluated by performing cell invasion assay using the Cultrex 3D Spheroid Cell Invasion Assay Kit (Trevigen) as per manufacturer's protocol. Briefly, control (3T3, C1, C2, C3, and C4) and 14-3-3 epsilon clones (EP1, EP3, EP10, EP11, EP12) were plated at a density of 3000 cells per well in 100 μl of 1× spheroid formation matrix (prepared in culture media) in a round bottom 96-well plate. Spheroids were allowed to form for 48 h and 100 μl of invasion matrix was added to each well to evaluate the invasiveness of the clones. Images of the spheroids were taken at 24 h intervals for 3 days. ImageJ was used to calculate the surface area of the spheroids at 0 and 72 h of invasion. Increase in the surface area was calculated relative to images taken before invasion matrix was added.

RESULTS

14-3-3 binds and colocalizes with DNMT1 post-DNA replication

To search for a reader of DNMT1pSer143 modification, we synthesized a biotin-tagged peptide encompassing the amino acids 132–150 of DNMT1 with phosphorylated Ser143 in the center and screened with a protein domain microarray, that harbored GST fusion proteins of 86 different phospho-serine/-threonine binding domains, to identify potential readers (24). The screen identified that the family of 14-3-3 proteins, including β, ϵ, γ, σ and ζ homologues, were able to bind the Ser143-phosphorylated peptide with varying affinities (Figure 1A). Furthermore, we performed an *in vitro* GST pull-down assay to establish that full-length DNMT1 and 14-3-3 proteins indeed interact. Purified GST-fusions of 14-3-3β, ϵ, γ, σ and ζ proteins were incubated separately with purified recombinant phosphorylated full-length DNMT1, and the pulled-down protein fraction was western blotted with anti-DNMT1 antibody. 14-3-3γ and β were the strongest binders among all homologues, although

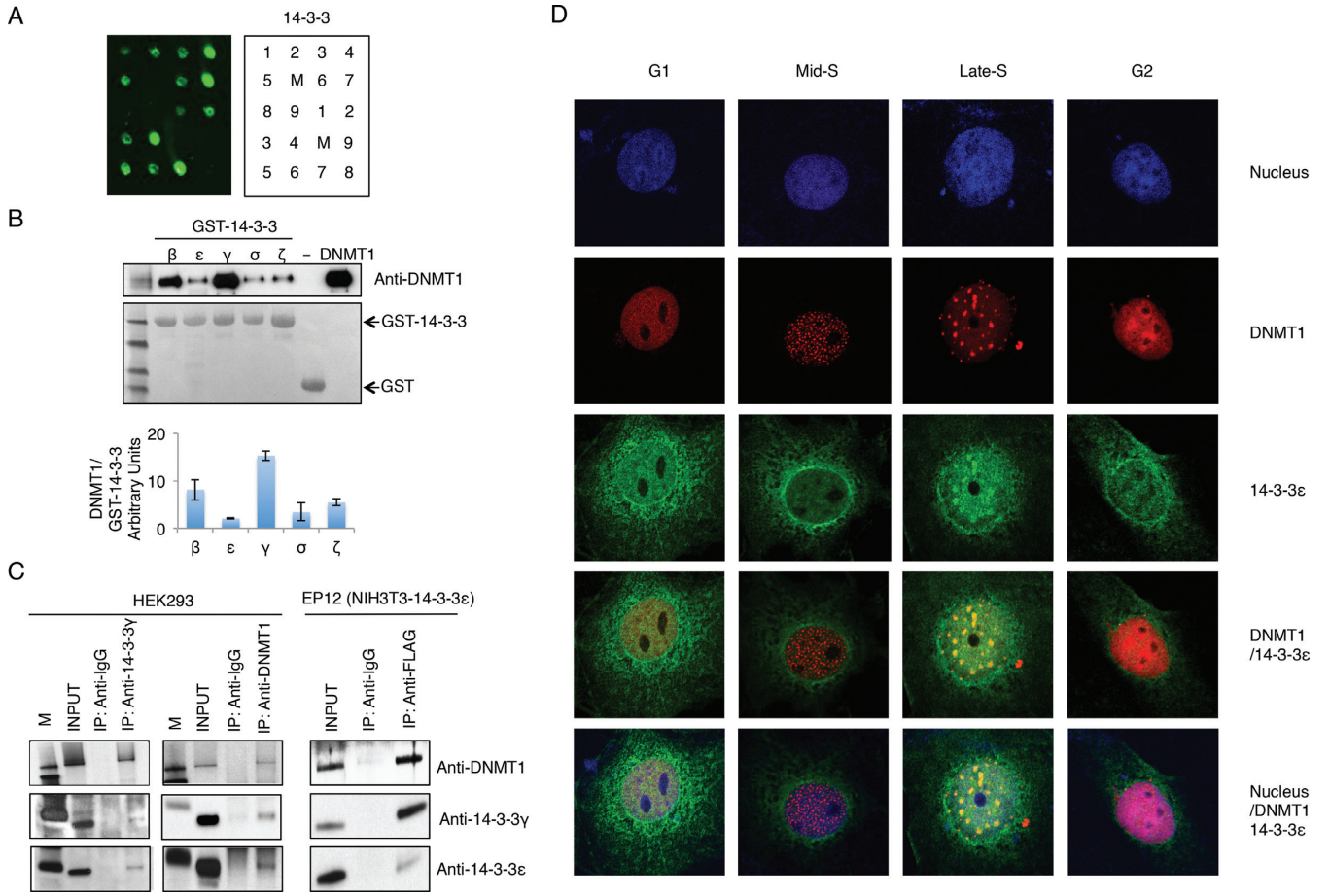

Figure 1. 14-3-3 binds and colocalizes with DNMT1. (**A**) Binding of DNMT1pSer143 peptide to a phospho-Serine/Threonine protein domain microarray to identify potential readers. The array contains the 14-3-3, 14-3-3-like, WW/SRI, BIR, POLO Box, MH2, WD40, FHA and BRCT domains fused to GST. Binding of biotin-tagged DNMT1pSer143 peptide to the array revealed 14-3-3 homologues as binding partners. The biotinylated peptide binding was detected using streptavidin –Cy3. An image of the full microarray is shown in Supplementary Figure S1A. (**B**) Recombinant full length DNMT1 binds different GST-14-3-3 homologues. Ponceau staining of transferred proteins from the GST pull-down are shown along with western blot using anti-DNMT1. Densitometry measurements of different 14-3-3 homologues binding to DNMT1 are shown at the bottom of the western blot (arbitrary units). **C**) Co-immunoprecipitations (Co-IP) of DNMT1 and 14-3-3γ and ϵ. Molecular weight marker, anti-DNMT1, anti-14-3-3γ, and anti-IgG antibodies, are indicated at the top of the western blots (left panel). Anti-FLAG antibody was used for 14-3-3ε immunoprecipitation in EP12 stable cell line overexpressing FLAG-14-3-3ϵ (right panel). Antibodies used for protein detection, anti-14-3-3γ, ϵ and anti-DNMT1, are indicated at the right side of the western blots. **D**) Colocalization studies between DNMT1 and 14-3-3ϵ. Plasmids encoding DsRed-DNMT1 (red) and FLAG-14-3-3ϵ (green) were co-transfected in COS7 cells. Different cell cycle phases are indicated on right side. DNA staining was performed using DAPI (blue). Yellow spots (merge) represent the colocalization.

others were also able to bind DNMT1 with different affinity (Figure 1B).

To validate if this interaction also occurs in cells, we performed co-immunoprecipitation and colocalization assays. In HEK293 cells immunoprecipitation (IP) with anti-14-3-3γ antibody was able to pull down DNMT1 along with 14-3-3ϵ. Reciprocal IP with anti-DNMT1 antibody was able to pull down 14-3-3ϵ and γ, but not by the control IgG antibody. The presence of both 14-3-3ϵ and γ suggested that DNMT1 might be able to bind both isoforms of 14-3-3 individually or as a heterodimer of 14-3-3γ and ϵ (Figure 1C, left panel). Further validation of 14-3-3ϵ and γ heterodimer interaction with cellular DNMT1 was tested in a NIH3T3 permanent cell line expressing FLAG-14-3-3ϵ. Immunoprecipitation using anti-FLAG antibody pulled down FLAG-14-3-3ϵ along with γ and DNMT1, confirming that DNMT1 also binds to heterodimer 14-3-3 species (Figure 1C, right panel).

We also validated the interaction between 14-3-3 proteins with DNMT1 by performing colocalization studies with 14-3-3 homologues, ϵ, β and γ. FLAG-14-3-3ϵ remained diffused throughout the cell, primarily cytoplasmic at G1, early and mid-S phase, but it displayed punctate nuclear pattern during late S-phase that colocalized with DsRed-DNMT1 (Figure 1D). During mid S-phase characteristic punctate pattern of colocalization between DsRed-DNMT1 and PCNA was observed, demonstrating replication coupled DNA methylation (36). Also, 14-3-3β and γ have similar nuclear colocalization with DNMT1 like that of 14-3-3ϵ (Supplementary Figure S1B). Although there was strong colocalization between 14-3-3 family proteins and DNMT1, a mutation of DNMT1S143A, that would abolish phosphorylation, resulted in poor colocalization

of 14-3-3β/DNMT1 and 14-3-3γ/DNMT1 in late S-phase (Supplementary Figure S2).

We also validated that punctate DsRed-DNMT1 indeed represents DNMT1pSer143 enzyme species by evaluating immunocolocalization signals between DsRed-DNMT1 and anti-DNMT1pSer143 in the absence or presence of pSer143 competitor peptide. The signal of DNMT1pSer143 was identical and overlapped with the DsRed-DNMT1 and the competitor peptide blocked antibody signal (Supplementary Figure S3A). Furthermore, mutation of DNMT1S143A abolished the overlapping signals between DNMT1pSer143 and DsRed-DNMT1S143A (Supplementary Figure S3B). Therefore, combined observations from GST pull-down, colocalization and co-immunoprecipitation of both DNMT1 and 14-3-3 homologues suggest a physical interaction between the two proteins.

The DNMT1 Lys142-Ser143 is analogous to some histone modification patterns—for example, the 'methyl-phospho' cassette of histone H3 Lys9 and Ser10 (37). The 14-3-3 proteins have been shown previously to bind Ser10-phosphorylated H3 peptides (38). The sequence similarity between DNMT1 (RS**KS**D**G**E) and H3 (AR**KS**T**G**G) suggested that 14-3-3 proteins contact the Ser143-phosphorylated DNMT1 peptide in the same manner as 14-3-3 contacts Ser10-phosphorylated H3 peptides (Supplementary Figure S4).

Phosphorylation dependent binding between 14-3-3 and DNMT1

14-3-3 proteins are known to bind a number of functionally diverse proteins that contain a phosphorylated serine or threonine residue. We therefore investigated if phosphorylation at Ser143 of DNMT1 is the primary determinant for binding to 14-3-3. Recombinant DNMT1 that is naturally phosphorylated at Ser143 (15) was treated with protein phosphatase PP1 that confers broad specificity towards phospho-serine/threonine. The PP1 treated and untreated DNMT1 was used for GST pull-down assay with 14-3-3γ. Increased concentration of untreated DNMT1 (phosphorylated in cell) showed a concentration dependent binding to 14-3-3γ whereas PP1 treated DNMT1 lost binding as revealed by anti-DNMT1pSer143 antibody (Figure 2A). Previously, we have identified AKT1 as the enzyme responsible for phosphorylation of Ser143 on DNMT1 (15). We therefore used AKT1 *in vitro* to phosphorylate GST fusion DNMT1 fragment encompassing the first 446 amino acids (GST-DNMT1 (1–446)) expressed and purified from *Escherichia coli* and performed binding experiments. Indeed, the phosphorylated GST-DNMT1 (1–446) showed robust binding to 14-3-3γ (Figure 2B). Since DNMT1pSer143 binds strongly to 14-3-3γ, we hypothesized that the DNMT1pSer143 in the complex would not be dephosphorylated by phosphatase PP1. To test our hypothesis, we incubated recombinant DNMT1 in the presence of 14-3-3γ first and then added PP1. As expected, PP1 was not able to dephosphorylate DNMT1pSer143 in the presence of 14-3-3γ *in vitro* (Figure 2C). To validate that 14-3-3 truly binds phosphorylated DNMT1 in the cell and blocks the phosphatase activity, we transfected 14-3-3ε, in the presence or absence of AKT1 and quantitated the phosphorylated DNMT1 in the cell extract. FLAG-14-3-3ε alone increased the level of DNMT1Ser143 phosphorylated species by two folds over FLAG control. Overexpression of AKT1 alone or AKT1 and 14-3-3ε also showed increased amounts of DNMT1pSer143 enzyme (Figure 2D). Furthermore, depletion of 14-3-3ε by siRNA led to decrease in DNMT1pSer143 species (Figure 2E). Therefore, the interactions between 14-3-3 and DNMT1pSer143 enzyme have profound effect on preservation of post-translational modification of DNMT1 or shield DNMT1pSer143 from dephosphorylation.

14-3-3 inhibits phosphorylated DNMT1Ser143 activity

We further examined if the binding of 14-3-3 with phosphorylated DNMT1 enzymes would have any effect on the DNA methyltransferase activity. Saturating amount of GST-14-3-3γ fusion protein or GST protein alone was incubated with either the full length DNMT1 or a truncated form lacking the amino-terminus 580 amino acids (DNMT1Δ580). The DNMT1 activity of these complexes was assayed in the presence of hemimethylated substrate DNA and tritiated AdoMet. The full-length DNMT1 showed drastic reduction of its activity (∼50%) in the presence of GST-14-3-3γ compared to GST alone. DNMT1 lacking the phosphorylated region (DNMT1Δ580) did not show significant loss of activity, suggesting 14-3-3γ binding impedes full-length DNMT1 activity (Figure 3A).

Since 14-3-3 impeded DNMT1 activity, and DNMT1–14-3-3 colocalization takes place following DNA replication, we attempted to understand the effect of their interaction on DNA methylation. Cell line overexpressing FLAG-14-3-3ε (EP12) was synchronized by double thymidine treatment. Cells were collected at various time points of cell cycle progression and DNA methyltransferase activity was measured using a hemimethylated oligonucleotide as a substrate. As the cells entered S-phase with active DNA synthesis, DNA methyltransferase activity increased (up to 10 h) and gradually decreased coinciding with end of DNA replication suggesting either degradation of DNMT1 or catalytic inactivation of DNMT1 (Figure 3B and C). A gradual increase and plateau of enzyme activity was observed post-DNA synthesis. Western blot of total DNMT1 input suggested steady amounts of DNMT1 throughout the cell cycle. Since high percentages of DNMT1 during DNA replication are phosphorylated (15), we hypothesized that inhibition of enzymatic activity is due to DNMT1pSer143–14-3-3 binary complex formation. To test our hypothesis, we cross-linked synchronized cells at various time points and immunoprecipitated 14-3-3 and probed the blot with DNMT1 and 14-3-3 antibodies (Figure 3B). Indeed, densitometry analysis demonstrated an increase in the formation of DNMT1 and 14-3-3 binary complexes between 10 and 16 h post release and peaked at 18 h, and this increased 14-3-3-DNMT1 binding inversely correlated with methyltransferase activity (Figure 3C). The input samples did not show increase in 14-3-3 or DNMT1 levels during the cell cycle (Figure 3B).

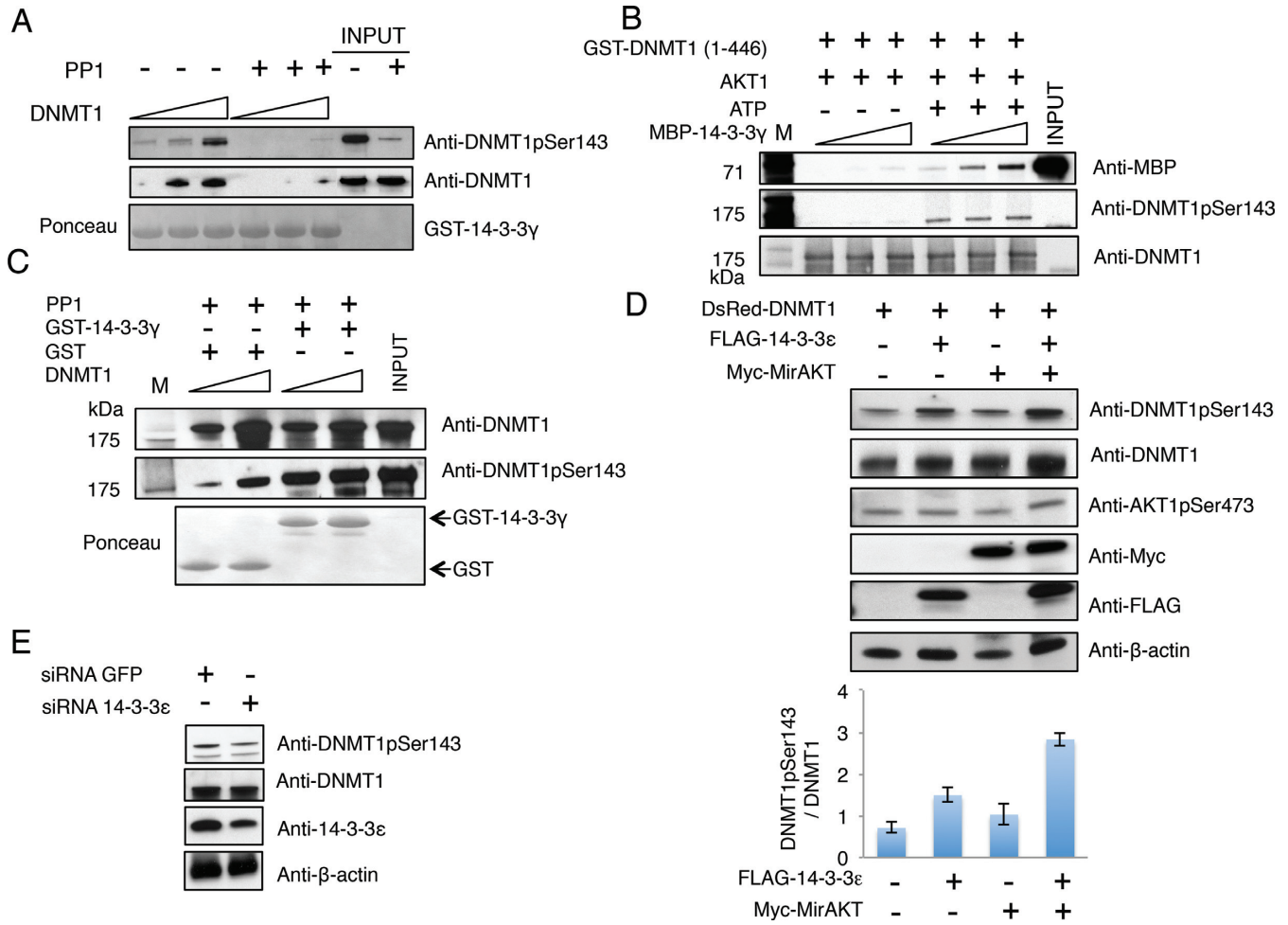

Figure 2. 14-3-3 protein bind and modulate phosphorylated DNMT1 levels. (**A**) Protein phosphatase 1 (PP1) impairs DNMT1 binding to GST-14-3-3γ. Presence (+) or absence (−) of PP1 with increasing amount of recombinant full-length DNMT1 (200, 400 or 600 ng) indicated on top of the western blots. Ponceau staining of transferred proteins from the GST pull-down are shown along with western blot using anti-DNMT1 or anti-DNMT1pSer143 antibody. (**B**) AKT1 kinase mediates DNMT1 binding to 14-3-3. GST-DNMT1 (1–446) phosphorylated (+, with ATP) or control (−, without ATP) with recombinant AKT1 kinase and incubated with different amounts of MBP-14-3-3γ recombinant protein is shown on top of the western blots. Antibodies against DNMT1, MBP and DNMT1pSer143 are indicated on the right side of the western blots. (**C**) 14-3-3 protein protect against DNMT1 dephosphorylation by PP1. Increasing amounts of recombinant full-length DNMT1 incubated with GST-14-3-3γ or control (GST) in presence of PP1 is shown at the top of the western blots. Ponceau staining of transferred proteins from the GST pull-down are shown along with western blot using anti-DNMT1 and anti-DNMT1pSer143. (**D**) Exogenous 14-3-3ε increases phosphorylation of DNMT1Ser143 by AKT1. Myc-MirAKT was transfected in COS7 cells in the presence (+) or absence (−) of 14-3-3ε as indicated on top. Antibodies used are indicated on the right side of the western blot. Densitometry analysis of DNMT1pSer143 was performed and shown as bar graphs below. (**E**) Depletion of 14-3-3ε by siRNA resulted in decrease DNMT1pSer143 protein. siRNA against GFP was used as the control. Antibodies used are indicated at the right side.

Overexpression of 14-3-3ε leads to aberrant DNA methylation

Overexpression of 14-3-3 in human carcinoma is well documented (39,40). Furthermore, aberrant DNA methylation of CpG islands and genome hypomethylation is a hallmark of various carcinomas. If 14-3-3 overexpression facilitates the impediment of DNMT1 activity, we hypothesized that this may result in aberrant DNA methylation and possibly hypomethylation of the genome. To test our hypothesis, we used synchronized permanent NIH3T3 cell lines expressing FLAG-14-3-3ε along with FLAG vector control. Overexpression of 14-3-3ε led to a significant decrease of DNMT1 specific activity (50%) post-DNA replication, while no changes of DNMT1 protein level was detected between clones overexpressing 14-3-3ε and clones expressing the vector control (Figure 4A). We then isolated genomic DNA from unsynchronized cells and performed nucleoside analysis to determine the global change in 5mC levels. Cell lines overexpressing 14-3-3ε were indeed hypomethylated (∼10% average 5mC methylation decrease in seven different clonal isolate) compared to the control cell lines (six different clonal isolate with control plasmid; Figure 4B, left panel). To rescue hypomethylated genome, we transfected EP10 or EP12 clone with wild-type *DNMT1* and performed global 5mC level analysis in the genomic DNA. Indeed, after two rounds of transfection both cell lines gained methylation similar to 5mC levels (∼3.5% of total C) as that of parental cell lines (Figure 4B, right panel). These results strongly suggest that the decrease in 5mC lev-

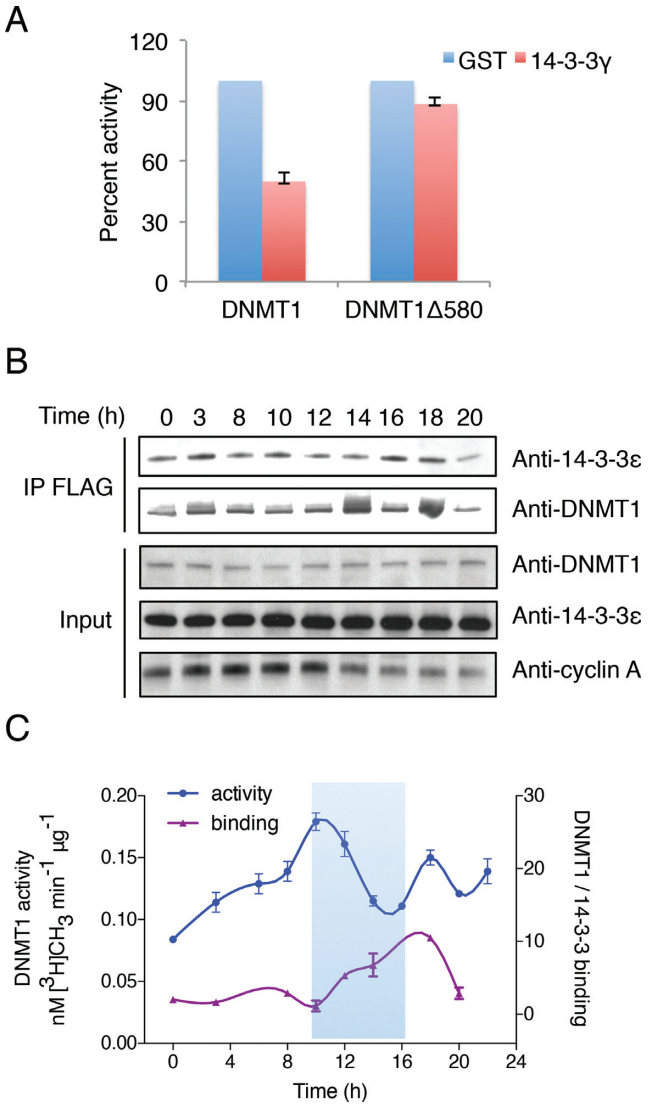

Figure 3. 14-3-3 proteins bind and inhibit phosphorylated DNMT1. (**A**) 14-3-3γ blocks activity of full-length DNMT1 and not DNMT1Δ580 *in vitro*. DNMT1 activity in the presence of GST (blue) or GST-14-3-3γ (red) is shown. (**B**) Western blot analysis of DNMT1–14-3-3 complexes after immunoprecipitation with anti-FLAG antibody during cell cycle. Synchronization timing after release is indicated on top. (**C**) Specific activity of DNMT1 and binding affinity of 14-3-3 and DNMT1 during cell cycle in 14-3-3 overexpression clone. Shaded region indicates the inverse correlation between increased 14-3-3-DNMT1 binding and DNMT1 methyltransferase activity.

els in 14-3-3 overexpressing clones is due to DNMT1 inhibition. We further performed reduced representation bisulfite sequencing (RRBS) to determine methylation changes between 14-3-3ε overexpressing and control genomes. Indeed, we identified about 11 000 differentially methylated regions (DMR), and the hypo versus hypermethylated ratio was about 2:1 (Figure 4C). Analysis of the genic region methylation between −5 kb transcription start and +5 kb transcription termination showed transcription start site and gene body hypomethylation in 14-3-3ε overexpressing clones (Figure 4D). The hypomethylation was pronounced in coding and intronic regions of the genes (Supplementary Figure S5). Similarly, CpG islands, particularly those in the promoter and gene body were also hypomethylated (Supplementary Figure S6). Overall all repetitive elements were hypomethylated (Figure 4E). Further analysis revealed that LINE, SINE and LTR elements were hypomethylated while satellites were hypermethylated (Supplementary Figure S7). These results suggest that 14-3-3 proteins can induce hypomethylation in general, and regional hypermethylation, which may influence gene expression.

14-3-3 activates tumorigenesis gene expression

Since the genome of 14-3-3ε overexpressing cell lines were hypomethylated in both CpG-island containing genes and repetitive DNA elements similar to cancer epigenome characteristics, we examined the transcription profile to determine the outcome of altered epigenome. Two individual 14-3-3 overexpressing clones (EP10 and EP12) were compared with two control clones (C2 and C3). Gene-wise dispersion analysis indicated good fitting of the expression values to the negative binomial distribution model used in RNA-seq data analysis (Supplementary Figure S8A). Also, clustering of the control and 14-3-3 overexpressed clones in different branches of the dendrogram generated using the Euclidean distance between samples indicated the successful differentiation of control and overexpressing clones using this model (Supplementary Figure S8B). The heat map between C2 and C3 or EP10 and EP12 were similar, suggesting clonal similarity of gene expression. However, comparison of gene expression between C2, C3 versus EP10, EP12 suggested significant differences (Supplementary Figure S9). Indeed, quantitative qPCR assay on selected genes validated the same trend of gene expression difference between 14-3-3ε overexpressing and control clones (Supplementary Figure S10). With adjusted p-value threshold of 0.01, we found 413 genes were upregulated and 252 genes were downregulated. The ratio between up and downregulated genes was about 2:1, correlating with hypo and hypermethylation of the genes (Figure 5A).

Gene ontology analysis suggested strong representation of cell migration and invasion pathway specific and facilitating genes, and among the upregulated genes the prominently enriched pathways were cell migration, mobility, proliferation and adhesion (Figure 5B). These multi-step processes play key roles in the progression of various diseases including cancer, atherosclerosis and arthritis. For example, one candidate gene in cell invasion pathway, Integrin-Linked Kinase (ILK) was overexpressed in 14-3-3 overexpressing cell lines. It has been documented that ILK overexpression indeed results in oncogenic transformation and progression to invasive and metastatic phenotypes (41).

Association of aberrant DNA methylation with differential gene expression

To demonstrate that the changes in gene expression observed with overexpression of 14-3-3 are due to, or partially resulting from companion aberrant DNA methylation, we correlated the gene expression data with DNA methylation data in the context of gene promoters and gene body. Log_2 fold change of gene expression values were correlated with

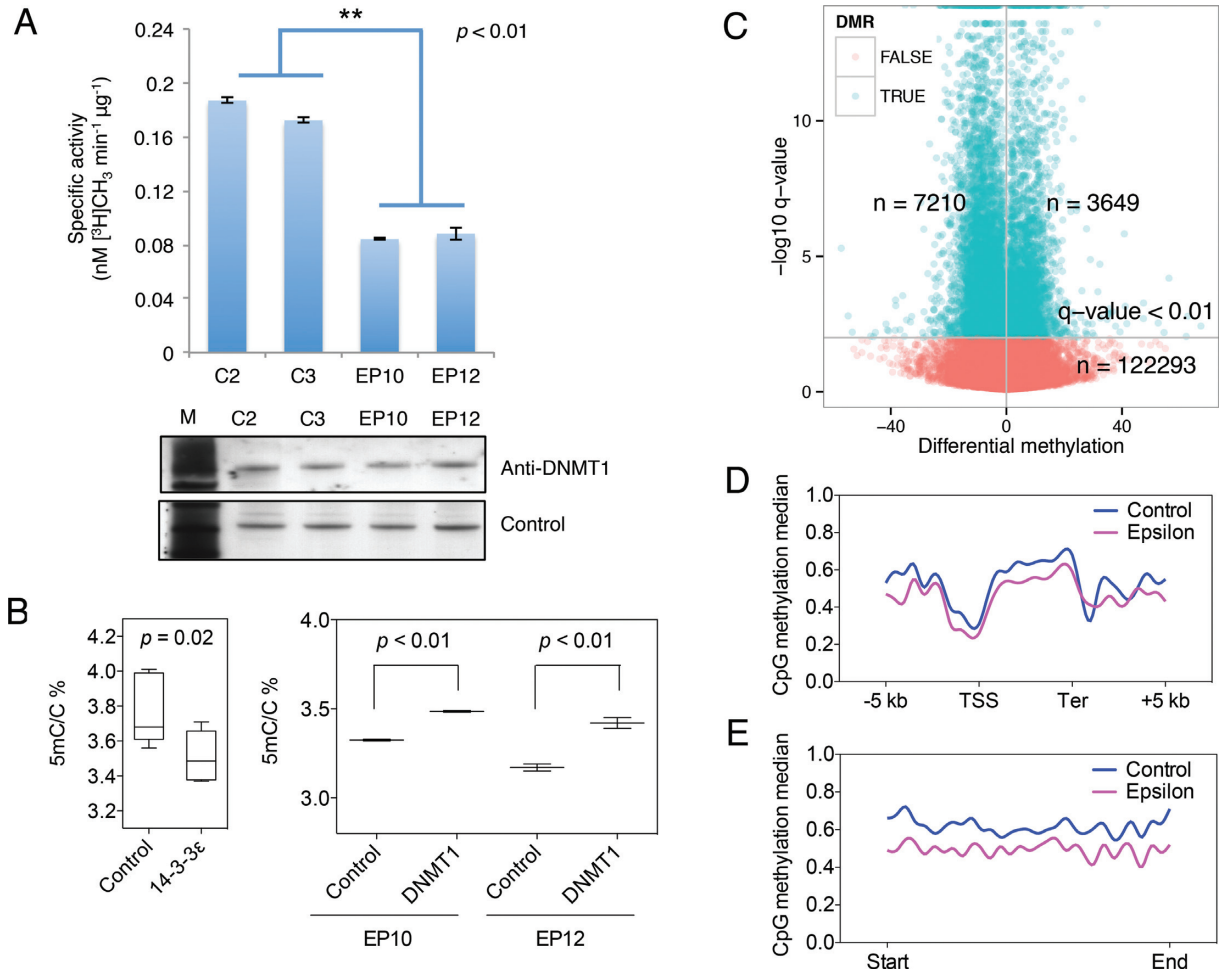

Figure 4. 14-3-3 overexpression hypomethylates genome. (**A**) DNA methylase assay showing reduced DNMT1 specific activity in NIH3T3 stable clonal cell lines overexpressing 14-3-3ϵ. Activity was measured from two control clones (C2 and C3) and two overexpressing clones (EP10 and EP12) using hemimethylated DNA substrate. Asterisk indicates *P* value less than 0.01 by *t*-test. Lower panel are western blots showing expression level of DNMT1 in the stable clones. (**B**) Global methylation level of stable clones measured by LC/MS (left). Data shown are from seven control clones and six 14-3-3ϵ stable clones. Global methylation level of stable clones transfected with full-length DNMT1 (right). *P* value is obtained by *t*-test. (**C**) Volcano plot showing the overall differential methylation profile of 5-kb tiles in the genome determined by RRBS. Differentially methylated region with a *q*-value < 0.01 are considered significantly different. (**D**) Differential methylation profile of genes (−5 kb transcription start site (TSS) to +5 kb transcription termination (Ter)). (**E**) Differential methylation profile of general genomic repetitive elements. Data shown are median value of two clones at each relative position (D and E).

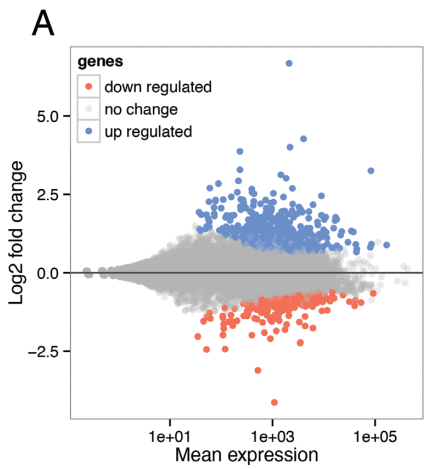

B

GO number	Term	Category	Background frequency	Sample frequency / input number	Expected	+/-	P-value
GO:0048583	regulation of response to stimulus	BP*	2735	114/413	47.03	+	5.19E-17
GO:0010646	regulation of cell communication	BP	2435	102/413	41.87	+	6.63E-15
GO:0072359	circulatory system development	BP	710	48/413	12.21	+	7.75E-13
GO:0030334	regulation of cell migration	BP	549	41/413	9.44	+	4.36E-12
GO:2000145	regulation of cell motility	BP	575	41/413	9.89	+	1.96E-11
GO:0042127	regulation of cell proliferation	BP	1281	59/413	22.03	+	4.40E-09
GO:0030335	positive regulation of cell migration	BP	321	27/413	5.52	+	1.56E-08
GO:0040017	positive regulation of locomotion	BP	346	28/413	5.95	+	1.60E-08
GO:2000147	positive regulation of cell motility	BP	329	27/413	5.66	+	2.68E-08
GO:0030198	extracellular matrix organization	BP	170	19/413	2.92	+	1.53E-07
GO:0005201	extracellular matrix structural constituent	MF*	37	8/413	0.64	+	7.16E-05
GO:0031012	extracellular matrix	CC*	394	45/413	6.78	+	4.76E-21
GO:0005925	focal adhesion	CC	335	22/413	5.76	+	1.76E-05

* BP, Biological process; MF, molecular function; CC, cellular components.

Figure 5. 14-3-3 overexpression affects gene expression. (**A**) MA plot of RNA-seq data showing upregulated (blue) and downregulated (red) genes. (**B**) Gene ontology analysis on upregulated genes.

differential CpG methylation levels in the promoter or gene body regions in the 14-3-3ε overexpression versus the vector control cell lines using Spearman's rank correlation and only genes showing significant expression change (adjusted *P*-value < 0.01) and significant CpG methylation change ($q < 0.05$) were included. The Spearman's rank correlation coefficients were -0.149 and -0.137 in the context of promoter and gene body, respectively. The Spearman's correlation coefficients and the p-value of correlation (0.026 and 0.003) indicate a significant negative association of gene expression with CpG methylation in the promoter and gene body region (Figure 6A).

We choose four genes that showed elevated expression in 14-3-3 overexpressed cell lines and examined their DNA methylation profile and correlated with gene expression. *Cxcl12*, chemokine (C-X-C Motif) ligand 12, functions as the ligand for the G-protein coupled receptor and participates in tumor growth and metastasis. We observed significant hypomethylation in 20 CpG sites at the 5′ of the transcript by an average of 26% and the gene expression level was increased ∼100-fold (Figure 6B, *Cxcl12*; Supplementary Figure S10). Similarly, *Synpo* gene encoding synaptopodin, an actin-associated protein that participates in actin-based cell shape formation and cell motility, was found significantly hypomethylated at seven CpG sites in the 5′ of the gene body by an average of 38% correlating with increased gene expression (Figure 6B, *Synpo*; Supplementary Figure S10). An adhesive glycoprotein thrombospondin 1 gene, *Thbs1*, that mediates cell-cell and cell-matrix interactions, was also found significantly hypomethylated in the 5′ of the gene body in four CpG sites by an average of 14% correlating with increased gene expression (Figure 6B, *Thbs1*; Supplementary Figure S10). Similarly, cell cycle progression gene, *Rgcc* involved in cell invasion (42), showed CpG hypomethylation across the promoter and gene body region. 15 CpG sites in the 5′ of the gene body showed an average demethylation of 36%, associated with an increased gene expression (Figure 6B, *Rgcc*; Supplementary Figure S10).

To unequivocally establish that *Cxcl12*, *Synpo*, *Rgcc*, *Dnaja4*, *Zhx1* and *Thbs1* gene expression is regulated by DNA methylation, we quantitated their expression levels in 5mC rescue experiment. Indeed, all the above genes that displayed higher expression in the presence of 14-3-3 were down regulated by DNMT1 transfection (Supplementary Figure S11). These data proves that additional DNMT1 in the cell can titer the 14-3-3 mediated DNMT1 inhibition and not only rescue DNA methylation, but also impose gene repression.

Genome hypomethylation and cell invasion in 14-3-3 overexpressed cell lines

Since 14-3-3ε overexpression leads to genomic hypomethylation, particularly on promoter and gene body of cell invasion specific genes and influenced their expression, we performed an *in vitro* cell invasion assay to determine its phenotypic effect. Parental cell line NIH3T3, four control (C1, C2, C3, C4) and five 14-3-3ε overexpressing cell lines (EP1, EP3, EP10, EP11, EP12) were chosen and 3D spheroid cell invasion assay was performed. Visual inspection of the spheroids showed extensive invasion by the 14-3-3ε overexpressing clones compared to the controls at 72 h in invasion matrix (Figure 7A). We observed a significantly higher increase in the surface area of the spheroids formed by 14-3-3ε overexpressing clones compared to either parent (3T3) or control cell lines (C1, C2, C3, and C4) (Figure 7B). These results supports the hypomethylation associated with invasion specific genes particularly in invasive spheroid.

Cancer tumors overexpresses 14-3-3

Cancer genome is known to be hypomethylated. Therefore, we investigated the correlation between 14-3-3 overexpression and various cancers by analyzing patient data from TCGA database (43). 14-3-3 homologues expression was altered in several major cancer types with either mutation or copy number variation and a majority of the changes representing increased copy numbers (Figure 8A). The percentile of patients with increased copy number of 14-3-3 ranges from 20% to 40% in uterine, ovarian, bladder, liver and breast cancer (Figure 8A). Remarkably, the alteration of 14-3-3 genes expression is significantly correlated with the reduced survival time of breast cancer patients (log-rank test, $P < 0.0043$, Figure 8B).

By detailed analysis, we observed that 14-3-3ζ was the most affected homologue in breast cancer patients with increased expression (Figure 8C). Thus, it is possible that increased 14-3-3 expressions could reduce CpG methylation in breast cancer by directly binding with DNMT1 and impacting DNA methyltransferase activity. When we correlated 14-3-3ζ expression (RNA-seq Ver2 data) with CpG methylation level of the major genomic elements (Illumina Infinium 450K array data) of the breast cancer patients, we found negative correlation between 14-3-3ζ expression levels to the DNA methylation level in LINE and LTR elements (Pearson's correlation, $p < 0.05$, Figure 8D and E). This observation is in agreement with our cell line data, in which we also observed that overexpression of 14-3-3ε resulted in LINE and LTR hypomethylation in NIH3T3 cells (Supplementary Figure S7).

DISCUSSION

Signaling pathways in mammalian cells are responsible for converting environmental cues into discrete intracellular events. The alteration of existing proteins by post-translational modification (PTM), such as serine or tyrosine phosphorylation is a key feature of signal-transduction pathways that allows the modulation of protein function affecting cellular processes (44). In mammalian nuclei the majority of epigenetic information are encoded in the chromatin and processed by well-choreographed post-translational modification of histones that changes chromatin structure and regulates gene expression. Extracellular signals for DNA damage or cell division induces histone phosphorylation. Phosphorylation of histones leads not only to the binding of specific reader proteins but also alters the affinity for readers or writers of other modifications. This allows crosstalk between different chromatin modifications for spatio-temporal control of chromatin-associated events (45). In the past years non-histone proteins, particularly pRB, ERα, p53, G9a and DNMT1 were

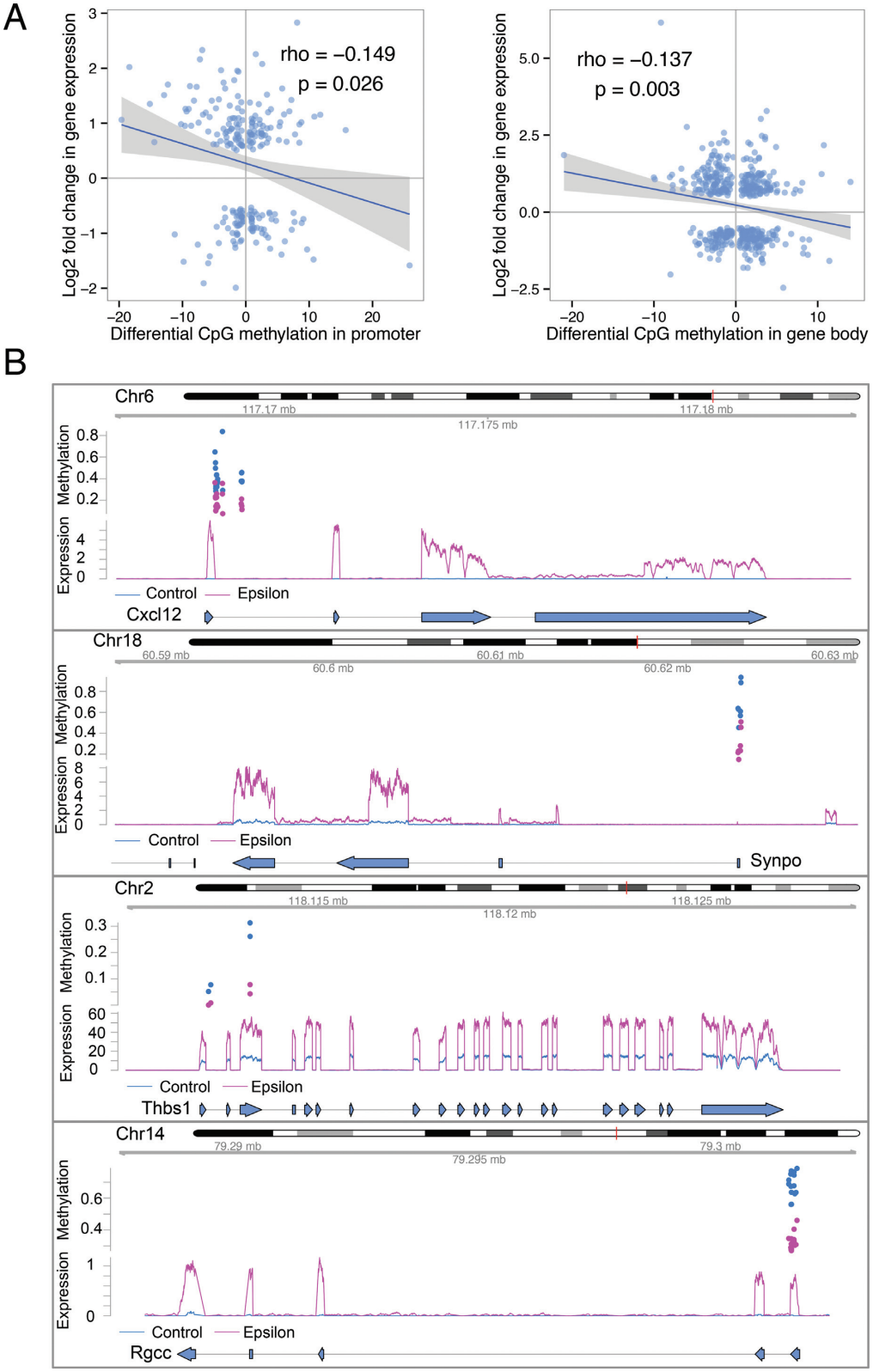

Figure 6. Correlation of promoter and gene body DNA hypomethylation with elevated gene expression. (**A**) Genome-wide correlation of DNA methylation and gene expression profile. Correlation analysis was carried out using Spearman's rank correlation test. A linear regression line was also drawn when plotting, and the shaded area represents the 95% confidential area of linear regression. Left, correlation of gene expression with promoter CpG methylation. Right, correlation of gene expression with gene body methylation. (**B**) CpG methylation (upper half) and gene expression (lower half) track of four representative genes displaying hypomethylation and elevated expression.

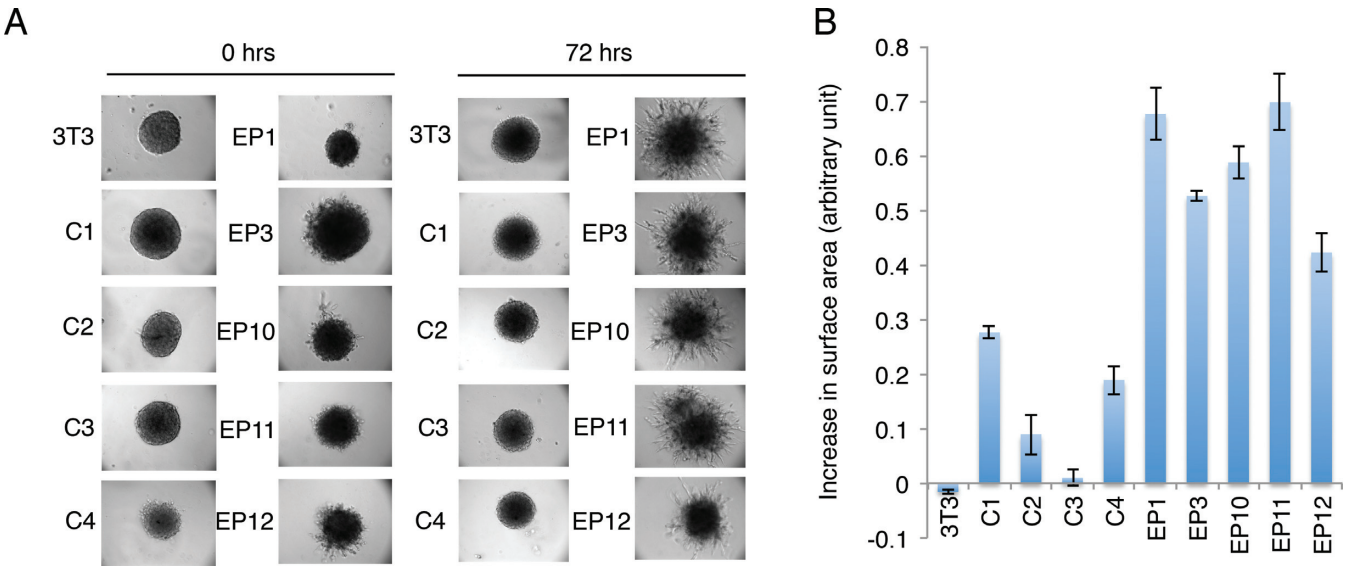

Figure 7. 14-3-3 overexpression promotes cell invasion. (**A**) Images of spheroids formed by control (3T3, C1, C2, C3 and C4) and 14-3-3ϵ overexpressing clones (EP1, EP3, EP10, EP11 and EP12) at 0 h of invasion (48 h post-seeding into spheroid formation matrix) are shown on the left and at 72 h of invasion on the right. (**B**) Quantitative presentation of increased surface areas of the spheroids at 0 and 72 hrs.

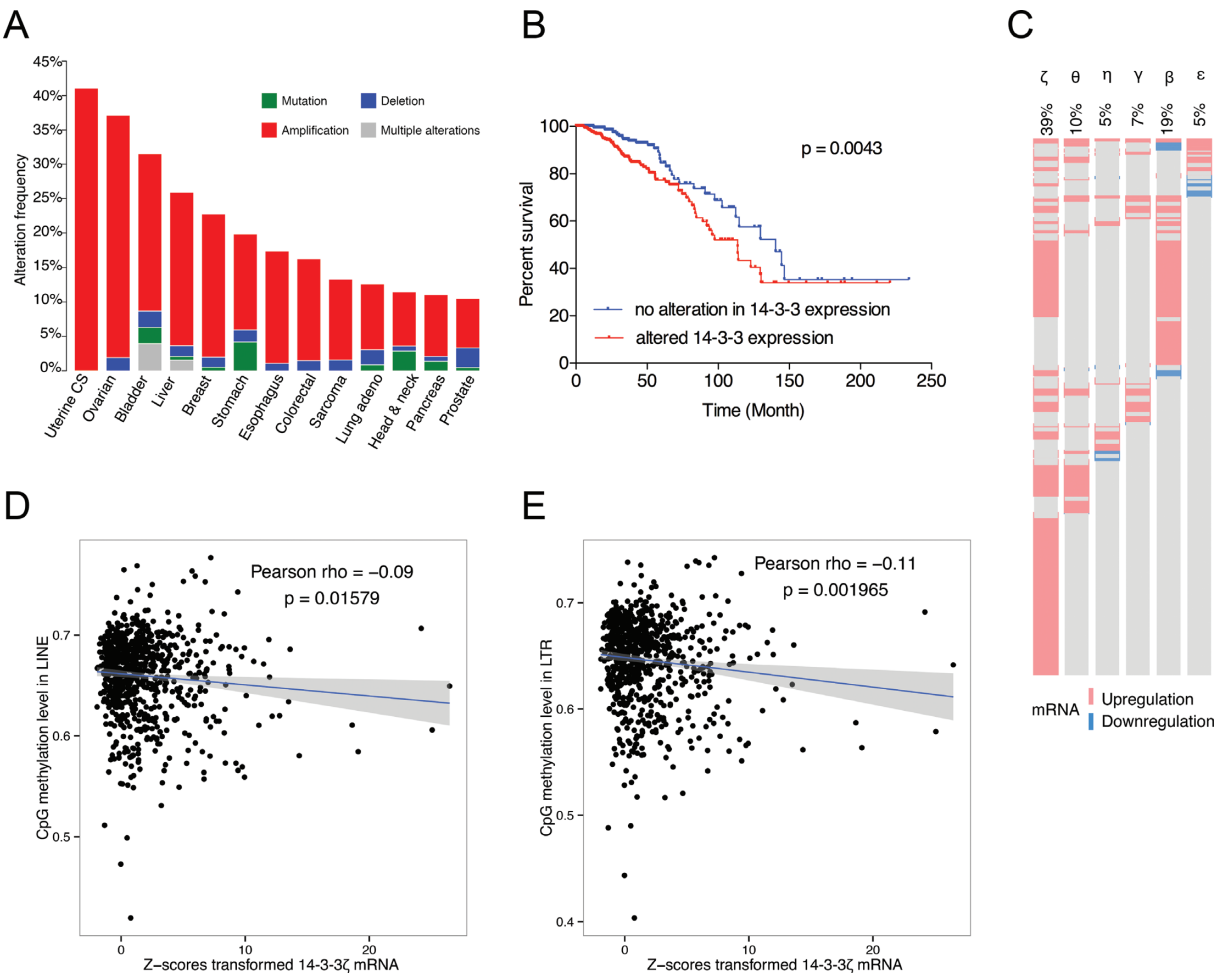

Figure 8. 14-3-3 overexpression is correlated with reduced patient survival time and repetitive elements hypomethylation in breast cancer. (**A**) Bar plot showing the frequency of 14-3-3 homologues alteration in major cancer types. (**B**) Kaplan–Meier curve showing the effect of 14-3-3 expression on the survival rates in breast cancer patients. (**C**) OncoPrint plot showing percentage of breast cancer patients with altered mRNA expression of 14-3-3 homologues. (**D** and **E**) Negative correlation of LINE and LTR methylation with 14-3-3ζ expression levels in breast cancer patients.

shown to be modified and their function regulated by post-translational modifications (15,46–48). For example, the unmodified status of pRb K810 in the conserved residue SPXK is essential for the recognition and phosphorylation of pRb by cyclin/Cdk. The lysine methyltransferase Set7/9 could methylate K810 and impede the binding of pRb with Cdk, which prevents phosphorylation of the associated serine residue and retain pRb in the growth-suppressing state (49). Indeed, the availability of the lysine residue for lysine methyltransferases can also be regulated by post-translational modifications at the residues surrounding the lysine residues (50).

A similar cross-talk between post-translational modifications of DNMT1 was observed previously. Methylation of K142 on DNMT1 by SET7 methyltransferase renders it to rapid ubiquitin-mediated degradation and this mechanism is blocked by phosphorylation of adjacent S143. The phosphorylated form of DNMT1 is abundant during DNA synthesis phase and is more stable compared to the K142 methylated DNMT1; suggesting that phosphorylation of DNMT1 may be a major event associated with maintenance of DNA methylation by DNMT1. Here we have discovered that 14-3-3 scaffold proteins are readers of DNMT1pSer143 and can influence its activity by binding. 14-3-3 proteins exist as homo or heterodimer in the cell and bind to DNMT1pSer143 species as a homo or heterodimer. Both 14-3-3 γ and ϵ were found to be immunoprecipitated with cellular DNMT1. Binding of 14-3-3 dimers is known to alter the conformation, prevent interaction, localization or accessibility of the target protein to other biological macromolecule. Indeed, in an *in vitro* DNA methyltransferase assay, addition of 14-3-3 to DNMT1 resulted in inhibition of its catalytic activity. Furthermore, crude extract from 14-3-3 overexpressing clones had diminished DNMT1 activity concurrent with a reduction in total 5mC in the genomic DNA. Overexpression of exogenous DNMT1 in 14-3-3 overexpressing clones resulted in rescue of 5mC content of the genome to comparable levels as observed in control clones, demonstrating a titration effect of 14-3-3 by additional DNMT1. In a recent study, CK2 was shown to phosphorylate endogenous DNMT3A at amino acids S386 and S389 located near its PWWP domain resulting in lowering of enzymatic activity for DNA methylation (16). The affected sequences are repetitive DNA, most notably Alu SINEs. Furthermore, CK2-mediated phosphorylation of DNMT3A is required for its heterochromatic localization (16). Therefore, both DNMT1 and DNMT3A activities may be regulated by cell signaling-mediated phosphorylation. To exclude the possibility that overexpression of 14-3-3 affects DNA methylation through modulating of DNMT3A/3B activities, we performed a sequence homology search using the consensus binding sequence of 14-3-3 ([A/R][R/S]KS[T/D]G[G/E]), and didn't discover any in DNMT3A or DNMT3B sequences. Thus it is probable that the regulation of DNA methylation by 14-3-3 is solely through its interaction with DNMT1. Since the rescue of DNA methylation occurred by exogenous DNMT1 expression, it is plausible that DNMT1 is the primary driver (Figure 4B).

Genomic DNA methylation analysis by RRBS of 14-3-3ϵ overexpressing clones suggested hypomethylation of genes that are essential for cell adhesion, migration, mobility and focal adhesion. Correlating well with hypomethylation of these genes, their transcription also increased, suggesting a mechanism of 14-3-3 mediated cell invasion by alteration of the epigenome. Indeed, epigenome alteration is associated with almost all carcinoma with a signature of global hypomethylation of the genome including the repetitive DNA. In a clinical study, seventy-one of 114 patients (62.3%) had a significant increase of 14-3-3ϵ expressions in hepatocellular carcinoma tissues, whereas normal tissues expressed weak or undetectable 14-3-3ϵ (51). In the same study, an elevated 14-3-3ϵ expression was significantly associated with shortened overall survival and progression-free survival. Furthermore, overexpression of 14-3-3ϵ increased the risk of metastasis by 4.6-fold (51). In another patient study, 14-3-3ϵ, ζ and θ were specifically expressed in meningioma, and their expression levels correlated with the increase of pathological grade of meningioma. Furthermore, 14-3-3ϵ, ζ and θ may be involved in tumorigenesis of meningioma and predictor for the degree of malignancy in meningioma (52).

Although the molecular mechanisms of 14-3-3-mediated carcinogenesis are poorly understood, there are multiple lines of evidence of their binding to various proteins with oncogenic potential, including member of Raf kinase family. In a SCID mice study, 14-3-3γ transfected NIH3T3 mouse fibroblast cells developed tumor and both MAP kinase and PI3K signaling pathways were shown to be essential for transformation (53). Altered interaction of 14-3-3 family of proteins in signaling pathways associated with cell proliferation, cell migration, and epithelial-to-mesenchymal transition can lead to tumorigenesis. In our study, we describe the changes in epigenome mediated by 14-3-3 scaffold proteins by directly modulating DNMT1 enzyme activity and thereby altering the transcription of key genes associated with cell invasion and cancer. These observations suggest a possible role of 14-3-3 proteins in altered cell signaling *via* regulation of DNMT1 activity leading to oncogenesis. Since 14-3-3 associates with multiple phosphorylated proteins, it could also work in a parallel pathway, inactivating repressors of gene expression, leading to changes in epigenome landscape and increased transcription, resulting in cell invasion and cancer.

ACCESSION NUMBER

RRBS data and RNA-seq data are available at Gene Expression Omnibus (GSE72860).

SUPPLEMENTARY DATA

Supplementary Data are available at NAR Online.

ACKNOWLEDGEMENT

We would like to thank Donald Comb, James V. Ellard, Rich Roberts, William Jack and Clotilde Carlow at New England Biolabs Inc., for research support and encouragement.

FUNDING

New England Biolabs Inc.; Cancer Prevention Research Institute of Texas [RP130432 to M.T.B.]; Center for Environ-

mental and Molecular Carcinogenesis at MD Anderson; X.C.'s laboratory was supported by NIH [GM049245-22]. Funding for open access charge: New England Biolabs Inc.
Conflict of interest statement. None declared.

REFERENCES

1. Hackett,J.A. and Surani,M.A. (2013) DNA methylation dynamics during the mammalian life cycle. *Philos. Trans. R. Soc. Lond. B Biol. Sci.*, **368**, 20110328.
2. Veitia,R.A., Veyrunes,F., Bottani,S. and Birchler,J.A. (2015) X chromosome inactivation and active X upregulation in therian mammals: facts, questions, and hypotheses. *J. Mol. Cell Biol.*, **7**, 2–11.
3. Ziller,M.J., Gu,H., Muller,F., Donaghey,J., Tsai,L.T., Kohlbacher,O., De Jager,P.L., Rosen,E.D., Bennett,D.A., Bernstein,B.E. *et al.* (2013) Charting a dynamic DNA methylation landscape of the human genome. *Nature*, **500**, 477–481.
4. Schoofs,T., Berdel,W.E. and Muller-Tidow,C. (2014) Origins of aberrant DNA methylation in acute myeloid leukemia. *Leukemia*, **28**, 1–14.
5. Hu,X.T. and He,C. (2013) Recent progress in the study of methylated tumor suppressor genes in gastric cancer. *Chin. J. Cancer*, **32**, 31–41.
6. Lopez-Serra,P. and Esteller,M. (2012) DNA methylation-associated silencing of tumor-suppressor microRNAs in cancer. *Oncogene*, **31**, 1609–1622.
7. Zhang,G. and Pradhan,S. (2014) Mammalian epigenetic mechanisms. *IUBMB Life*, **66**, 240–256.
8. Bostick,M., Kim,J.K., Estève,P.O., Clark,A., Pradhan,S. and Jacobsen,S.E. (2007) UHRF1 plays a role in maintaining DNA methylation in mammalian cells. *Science*, **317**, 1760–1764.
9. Butler,J.S., Lee,J.H. and Skalnik,D.G. (2008) CFP1 interacts with DNMT1 independently of association with the Setd1 Histone H3K4 methyltransferase complexes. *DNA Cell Biol.*, **27**, 533–543.
10. Bourc'his,D., Xu,G.L., Lin,C.S., Bollman,B. and Bestor,T.H. (2001) Dnmt3L and the establishment of maternal genomic imprints. *Science*, **294**, 2536–2539.
11. Sharif,J., Muto,M., Takebayashi,S., Suetake,I., Iwamatsu,A., Endo,T.A., Shinga,J., Mizutani-Koseki,Y., Toyoda,T., Okamura,K. *et al.* (2007) The SRA protein Np95 mediates epigenetic inheritance by recruiting Dnmt1 to methylated DNA. *Nature*, **450**, 908–912.
12. Leonhardt,H., Page,A.W., Weier,H.U. and Bestor,T.H. (1992) A targeting sequence directs DNA methyltransferase to sites of DNA replication in mammalian nuclei. *Cell*, **71**, 865–873.
13. Di Ruscio,A., Ebralidze,A.K., Benoukraf,T., Amabile,G., Goff,L.A., Terragni,J., Figueroa,M.E., De Figueiredo Pontes,L.L., Alberich-Jorda,M., Zhang,P. *et al.* (2013) DNMT1-interacting RNAs block gene-specific DNA methylation. *Nature*, **503**, 371–376.
14. Zhang,G., Estève,P.O., Chin,H.G., Terragni,J., Dai,N., Correa,I.R. Jr and Pradhan,S. (2015) Small RNA-mediated DNA (cytosine-5) methyltransferase 1 inhibition leads to aberrant DNA methylation. *Nucleic Acids Res.*, **43**, 6112–6124.
15. Estève,P.O., Chang,Y., Samaranayake,M., Upadhyay,A.K., Horton,J.R., Feehery,G.R., Cheng,X. and Pradhan,S. (2011) A methylation and phosphorylation switch between an adjacent lysine and serine determines human DNMT1 stability. *Nat. Struct. Mol. Biol.*, **18**, 42–48.
16. Deplus,R., Blanchon,L., Rajavelu,A., Boukaba,A., Defrance,M., Luciani,J., Rothe,F., Dedeurwaerder,S., Denis,H., Brinkman,A.B. *et al.* (2014) Regulation of DNA methylation patterns by CK2-mediated phosphorylation of Dnmt3a. *Cell Rep.*, **8**, 743–753.
17. Deplus,R., Denis,H., Putmans,P., Calonne,E., Fourrez,M., Yamamoto,K., Suzuki,A. and Fuks,F. (2014) Citrullination of DNMT3A by PADI4 regulates its stability and controls DNA methylation. *Nucleic Acids Res.*, **42**, 8285–8296.
18. Johnson,L.N. and Barford,D. (1993) The effects of phosphorylation on the structure and function of proteins. *Annu. Rev. Biophys. Biomol. Struct.*, **22**, 199–232.
19. Dalal,S.N., Schweitzer,C.M., Gan,J. and DeCaprio,J.A. (1999) Cytoplasmic localization of human cdc25C during interphase requires an intact 14-3-3 binding site. *Mol. Cell. Biol.*, **19**, 4465–4479.
20. Cann,K.L. and Hicks,G.G. (2007) Regulation of the cellular DNA double-strand break response. *Biochem. Cell Biol.*, **85**, 663–674.
21. Winter,S., Simboeck,E., Fischle,W., Zupkovitz,G., Dohnal,I., Mechtler,K., Ammerer,G. and Seiser,C. (2008) 14-3-3 proteins recognize a histone code at histone H3 and are required for transcriptional activation. *EMBO J.*, **27**, 88–99.
22. Estève,P.O., Chin,H.G., Benner,J., Feehery,G.R., Samaranayake,M., Horwitz,G.A., Jacobsen,S.E. and Pradhan,S. (2009) Regulation of DNMT1 stability through SET7-mediated lysine methylation in mammalian cells. *Proc. Natl. Acad. Sci. U.S.A.*, **106**, 5076–5081.
23. Estève,P.O., Terragni,J., Deepti,K., Chin,H.G., Dai,N., Espejo,A., Correa,I.R. Jr, Bedford,M.T. and Pradhan,S. (2014) Methyllysine reader plant homeodomain (PHD) finger protein 20-like 1 (PHF20L1) antagonizes DNA (cytosine-5) methyltransferase 1 (DNMT1) proteasomal degradation. *J. Biol. Chem.*, **289**, 8277–8287.
24. Espejo,A., Cote,J., Bednarek,A., Richard,S. and Bedford,M.T. (2002) A protein-domain microarray identifies novel protein–protein interactions. *Biochem. J.*, **367**, 697–702.
25. Pradhan,S., Bacolla,A., Wells,R.D. and Roberts,R.J. (1999) Recombinant human DNA (cytosine-5) methyltransferase. I. Expression, purification, and comparison of de novo and maintenance methylation. *J. Biol. Chem.*, **274**, 33002–33010.
26. Andrews,N.C. and Faller,D.V. (1991) A rapid micropreparation technique for extraction of DNA-binding proteins from limiting numbers of mammalian cells. *Nucleic Acids Res.*, **19**, 2499.
27. Estève,P.O., Chin,H.G., Smallwood,A., Feehery,G.R., Gangisetty,O., Karpf,A.R., Carey,M.F. and Pradhan,S. (2006) Direct interaction between DNMT1 and G9a coordinates DNA and histone methylation during replication. *Genes Dev.*, **20**, 3089–3103.
28. Meissner,A., Gnirke,A., Bell,G.W., Ramsahoye,B., Lander,E.S. and Jaenisch,R. (2005) Reduced representation bisulfite sequencing for comparative high-resolution DNA methylation analysis. *Nucleic Acids Res.*, **33**, 5868–5877.
29. Krueger,F. and Andrews,S.R. (2011) Bismark: a flexible aligner and methylation caller for Bisulfite-Seq applications. *Bioinformatics*, **27**, 1571–1572.
30. Akalin,A., Kormaksson,M., Li,S., Garrett-Bakelman,F.E., Figueroa,M.E., Melnick,A. and Mason,C.E. (2012) methylKit: a comprehensive R package for the analysis of genome-wide DNA methylation profiles. *Genome Biol.*, **13**, R87.
31. Quinlan,A.R. and Hall,I.M. (2010) BEDTools: a flexible suite of utilities for comparing genomic features. *Bioinformatics*, **26**, 841–842.
32. Kim,D., Pertea,G., Trapnell,C., Pimentel,H., Kelley,R. and Salzberg,S.L. (2013) TopHat2: accurate alignment of transcriptomes in the presence of insertions, deletions and gene fusions. *Genome Biol.*, **14**, R36.
33. Love,M.I., Huber,W. and Anders,S. (2014) Moderated estimation of fold change and dispersion for RNA-seq data with DESeq2. *Genome Biol.*, **15**, 550.
34. Anders,S., Pyl,P.T. and Huber,W. (2015) HTSeq-a Python framework to work with high-throughput sequencing data. *Bioinformatics*, **31**, 166–169.
35. Carbon,S., Ireland,A., Mungall,C.J., Shu,S., Marshall,B. and Lewis,S. (2009) AmiGO: online access to ontology and annotation data. *Bioinformatics*, **25**, 288–289.
36. Chuang,L.S., Ian,H.I., Koh,T.W., Ng,H.H., Xu,G. and Li,B.F. (1997) Human DNA-(cytosine-5) methyltransferase-PCNA complex as a target for p21WAF1. *Science*, **277**, 1996–2000.
37. Fischle,W., Wang,Y. and Allis,C.D. (2003) Binary switches and modification cassettes in histone biology and beyond. *Nature*, **425**, 475–479.
38. Macdonald,N., Welburn,J.P., Noble,M.E., Nguyen,A., Yaffe,M.B., Clynes,D., Moggs,J.G., Orphanides,G., Thomson,S., Edmunds,J.W. *et al.* (2005) Molecular basis for the recognition of phosphorylated and phosphoacetylated histone H3 by 14-3-3. *Mol. Cell*, **20**, 199–211.
39. Zhao,G.Y., Ding,J.Y., Lu,C.L., Lin,Z.W. and Guo,J. (2014) The overexpression of 14-3-3zeta and Hsp27 promotes non-small cell lung cancer progression. *Cancer*, **120**, 652–663.
40. Zhang,Y., Li,Y., Lin,C., Ding,J., Liao,G. and Tang,B. (2014) Aberrant upregulation of 14-3-3sigma and EZH2 expression serves as an inferior prognostic biomarker for hepatocellular carcinoma. *PLoS One*, **9**, e107251.
41. Legate,K.R. and Fassler,R. (2009) Mechanisms that regulate adaptor binding to beta-integrin cytoplasmic tails. *J. Cell Sci.*, **122**, 187–198.
42. Fosbrink,M., Cudrici,C., Niculescu,F., Badea,T.C., David,S., Shamsuddin,A., Shin,M.L. and Rus,H. (2005) Overexpression of

RGC-32 in colon cancer and other tumors. *Exp. Mol. Pathol.*, **78**, 116–122.
43. Weinstein,J.N., Collisson,E.A., Mills,G.B., Shaw,K.R., Ozenberger,B.A., Ellrott,K., Shmulevich,I., Sander,C. and Stuart,J.M. (2013) The Cancer Genome Atlas Pan-Cancer analysis project. *Nat. Genet.*, **45**, 1113–1120.
44. Graves,J.D. and Krebs,E.G. (1999) Protein phosphorylation and signal transduction. *Pharmacol. Ther.*, **82**, 111–121.
45. Rossetto,D., Avvakumov,N. and Cote,J. (2012) Histone phosphorylation: a chromatin modification involved in diverse nuclear events. *Epigenetics*, **7**, 1098–1108.
46. Macdonald,J.I. and Dick,F.A. (2012) Posttranslational modifications of the retinoblastoma tumor suppressor protein as determinants of function. *Genes Cancer*, **3**, 619–633.
47. Le Romancer,M., Poulard,C., Cohen,P., Sentis,S., Renoir,J.M. and Corbo,L. (2011) Cracking the estrogen receptor's posttranslational code in breast tumors. *Endocr. Rev.*, **32**, 597–622.
48. Huang,J., Perez-Burgos,L., Placek,B.J., Sengupta,R., Richter,M., Dorsey,J.A., Kubicek,S., Opravil,S., Jenuwein,T. and Berger,S.L. (2006) Repression of p53 activity by Smyd2-mediated methylation. *Nature*, **444**, 629–632.
49. Carr,S.M., Munro,S., Kessler,B., Oppermann,U. and La Thangue,N.B. (2011) Interplay between lysine methylation and Cdk phosphorylation in growth control by the retinoblastoma protein. *EMBO J.*, **30**, 317–327.
50. Binda,O. (2013) On your histone mark, SET, methylate! *Epigenetics*, **8**, 457–463.
51. Ko,B.S., Chang,T.C., Hsu,C., Chen,Y.C., Shen,T.L., Chen,S.C., Wang,J., Wu,K.K., Jan,Y.J. and Liou,J.Y. (2011) Overexpression of 14-3-3epsilon predicts tumour metastasis and poor survival in hepatocellular carcinoma. *Histopathology*, **58**, 705–711.
52. Liu,Y., Tian,R.F., Li,Y.M., Liu,W.P., Cao,L., Yang,X.L., Cao,W.D. and Zhang,X. (2010) The expression of seven 14-3-3 isoforms in human meningioma. *Brain Res.*, **1336**, 98–102.
53. Radhakrishnan,V.M. and Martinez,J.D. (2010) 14-3-3gamma induces oncogenic transformation by stimulating MAP kinase and PI3K signaling. *PLoS One*, **5**, e11433.